Phase diagram of Li_xC_6

J. R. Dahn
Department of Physics, Simon Fraser University, Burnaby, British Columbia, Canada V5A 1S6
(Received 28 June 1991)

Using lithium/graphite electrochemical cells and *in situ* x-ray diffraction, we have determined the phase diagram of Li_xC_6 for $0<x<1$ and $0\,°C<T<70\,°C$. We find several differences between our results and previous work. For $x<0.04$, the intercalated Li is randomly distributed throughout the graphite host in a dilute stage-1 phase. As x increases past 0.04, a clear coexistence between this phase and a stage-4 phase is observed. As x increases further at 21 °C, transitions to stage 3, to a "liquidlike" stage-2 phase (denoted $2L$), to stage 2, and finally to filled stage 1 occur sequentially as expected on the basis of previous work. We have been able to accurately determine the ranges in x and in T of the single-phase and the coexisting-phase regions. Clear coexisting-phase regions are observed (indicating first-order transitions) for all the transitions except for the stage-4 to -3 transition. We discuss the difference between this transition and the others. The average layer spacing of Li_xC_6 has been measured as a function of x.

INTRODUCTION

The intercalation of lithium in graphite and studies of the staged phases which form have been extensively studied both theoretically and experimentally.[1-5] More recently, experiments have focused on the determination of the phase diagram of the staged phases[5-10] using samples prepared chemically having fixed overall composition. The sample temperature is varied and the structure is probed using diffraction methods to determine the phases present. The phase diagram is determined by combining the phase-temperature results from numerous samples having different Li concentration x in Li_xC_6.

Phase diagrams of Li intercalation compounds are well probed using electrochemical methods and *in situ* x-ray diffraction.[11,12] Electrochemical cells are used to intercalate Li into graphite at a fixed temperature and the voltage of these cells is used to measure the chemical potential of the intercalated Li.[13] Because the chemical potential of Li in coexisting phases is equal, coexisting phase regions appear as plateaus in plots of the voltage $V(x,T)$ of Li/Li_xC_6 cells versus x at fixed temperature T. The derivative, $-(dx/dV)_T$, shows peaks at the voltages and compositions where coexisting phases occur. Structural information is simultaneously acquired using cells with Be x-ray windows.[14] Phase diagrams are determined by combing the results obtained during a number of fixed temperature intercalations.

Early attempts to intercalate Li into graphite using electrochemical cells[15-17] have been plagued with side reactions (caused by electrolyte decomposition) and therefore are not reliable measurements of the chemical potential variation. Recently, we learned how to overcome these experimental difficulties[18,19] and studied the intercalation of Li within disordered carbons.[20] In Ref. 20 we reported preliminary studies on Li intercalated graphite which showed that the coexisting phase regions between the staged phases in Li_xC_6 were easily observed in $V(x,T)$ and $-(dx/dV)_T$. Here we concentrate entirely on an accurate determination of the phase diagram of Li intercalated graphite in the temperature range ($0\,°C<T<70\,°C$) accessible to our electrochemical cells.

EXPERIMENT

Crystalline synthetic graphite powder (99.9% pure), designated KS-44, was obtained from Lonza Corporation. The mean particle size of this powder is 44 μm and the spacing between (002) planes, $d(002)$, is 3.355 Å indicative of well-graphitized material.[21] Electrodes were prepared from this powder as described previously.[20] In some electrodes we added 7% by weight of Super S Battery Black (Chemetals Inc. Baltimore Md., USA) a carbon black which ensures good electrical contact between particles in the electrode. Super S black reversibly intercalates about $\Delta x=\frac{1}{2}$ in Li_xC_6.[22] For the Li/(Super S Battery Black) cells described in Ref. 22, $V(x,T)$ varies almost linearly from $x=0$ at $V=1.4$ V to $x=0.5$ at $V=0.01$ V. Thus, for cells containing Super S Battery Black, we must remember that a small fraction of the total Li ($0.5\times0.07/(1\times0.93)=0.037$) is intercalating into the Super S Battery Black, not into the graphite.

Two electrode electrochemical cells were constructed using the electrodes described above, Li foil (Lithium Corporation of America), porous polypropylene separators (Celgard 2502 from Celanese Corp.), and a nonaqueous electrolyte containing a dissolved Li salt and a sequestering agent which prevents the cointercalation of the electrolyte solvent along with the Li atom.[19] The electrolyte was a $1M$ solution of $LiN(CF_3SO_2)_2$ (3M Corporation) and 12-crown-4 ether (Aldrich Chemical Co.) dissolved in a 50:50 volume mixture of propylene carbonate and ethylene carbonate (Texaco). The salt was vacuum dried at 140 °C and the solvents were vacuum

distilled prior to use. The 12-crown-4 ether was used as received. The moisture content of the electrolyte was less than 100 ppm.

Two types of electrochemical cells were used here. Hermetically sealed test cells of the type described in Ref. 18 were used to determine $V(x,T)$ of Li/Li_xC_6 cells. Electrochemical cells with Be x-ray windows[14] were used so that structural changes in the intercalated graphite could be measured *in situ* as x in Li_xC_6 is changed by charging or discharging the cells. Our diffractometer uses Cu $K\alpha$ radiation.

To determine $V(x,T)$ and $-dx/dV$, cells were charged and discharged using constant currents between fixed voltage limits. The temperature of the cell was maintained constant in a thermostat to $\pm 0.1\,^{\circ}C$. The cell cyclers maintain stable currents to $\pm 0.5\%$. Changes in x are calculated from the cathode mass, the constant current, and the time of current flow. Data were measured whenever V changed by ± 0.001 V. For the *in situ* diffraction experiment, cells were equilibrated at fixed voltage using a Princeton Applied Research 273 potentiostat; once the cell current fell below 1 μA, x-ray scans were measured. The value of x corresponding to each scan was then obtained from the cell voltage and $V(x)$ measured on a different cell using a current corresponding to a change $\Delta x = 1$ in 800 h (for a typical cell with 15-mg graphite, this current is 6.9 μA). X-ray profiles were collected at 66 voltages over a period of about 2 months while the voltage of the cell was gradually stepped down (intercalating Li) and then gradually stepped back up again (deintercalating Li).

The x-ray experiment is used to identify the phase transitions corresponding to the various plateaus in $V(x,T)$ and the peaks in $-dx/dV$. Then, we extract the phase diagram from the compositions corresponding to the beginning and the end of each plateau. These compositions can often be determined directly from $V(x)$, but are sometimes more easily observed when $-dx/dV$ is plotted versus x.

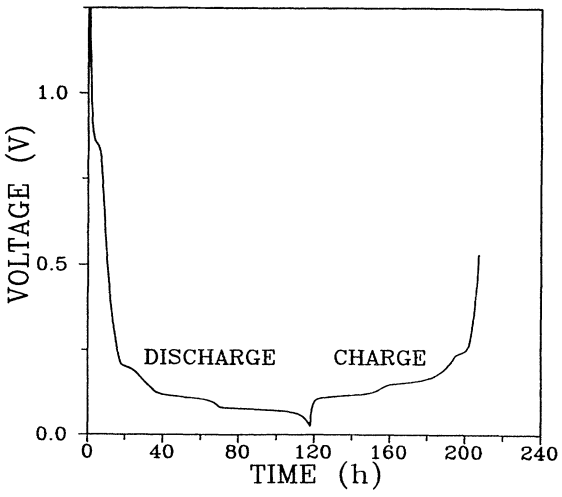

FIG. 1. Voltage vs time for the first discharge and charge of a Li/graphite cell at 30 °C. The currents used correspond to a change $\Delta x = 1$ in Li_xC_6 in 100 h.

RESULTS

Figure 1 shows the first discharge and charge of a Li/graphite cell using a current corresponding to a change $\Delta x = 1$ in 100 h. The graphite electrode in this cell contained 7% by weight of Super S Battery Black. The plateau near 0.85 V is associated with the decomposition of the electrolyte on the surface of the carbons in the formation of a passivating layer.[18] This plateau is not observed on subsequent cycles because once the passivating layer is formed, it protects the lithiated carbon from further reaction. The other plateaus below 0.52 V each correspond to a transition between staged phases of different composition. For example, in our previous work,[20] we showed that the lowest voltage plateau (near

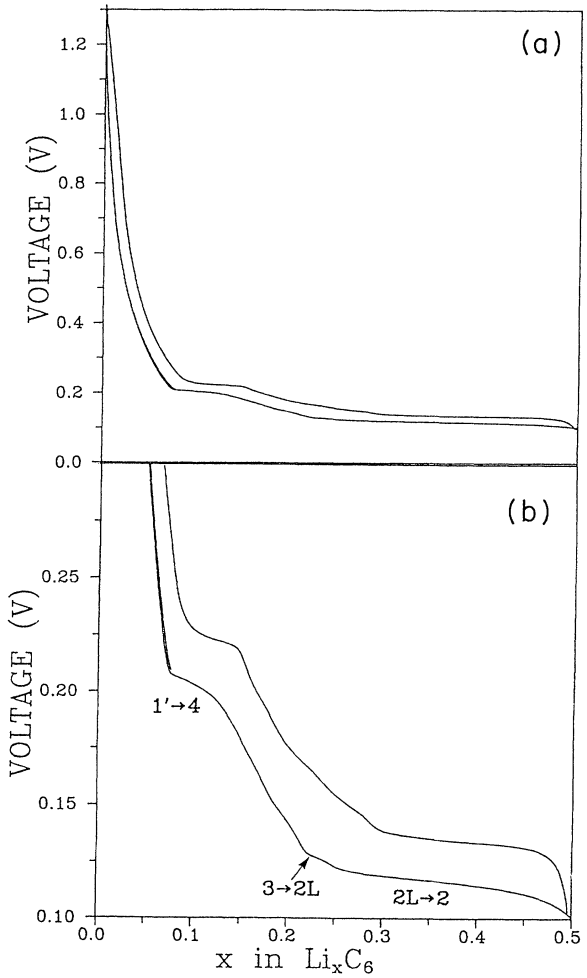

FIG. 2. Voltage vs x for a Li/graphite cell measured at 30 °C using currents corresponding to a change $\Delta x = 1$ in Li_xC_6 in 800 h. The lower curve in (a) and in (b) is for the discharge of the cell and the upper curve is for the charge. The correspondence between the plateaus in $V(x,T)$ and transitions between the staged phases has been indicated for the discharge.

70 mV during discharge) corresponds to the stage-2–stage-1 coexistence region. The discharge of the cell took longer than the subsequent charge because the electrolyte decomposition associated with the formation of the passivating film consumes Li which has been transferred to the graphite electrode. Although this process is clearly evident at 0.85 V, it occurs slowly throughout the rest of the first discharge.

Figure 2 shows the second discharge-charge cycle of a Li/graphite cell at 30 °C using currents corresponding to an 800-h rate. The cell was discharged only to 0.1 V, which corresponds to $x = 0.5$, and then charged. Had the cell been allowed to discharge further, to 0.02 V, another plateau extending from $x = \frac{1}{2}$ to 1 would have been observed.[20] Figure 2(b) clearly shows the plateaus which mark coexisting phase regions. We have labeled the plateaus on discharge based on the x-ray work to be presented below. The offset between the charge and discharge is due to the IR drop from the internal resistance of the cell. If the cell could be measured under truly equilibrium conditions, $V(x,T)$ would lie midway between the charge and discharge data shown.

Figure 3 shows $-(dx/dV)_T$ calculated from the data of Fig. 2. The derivative is obtained simply by taking $\Delta x/\Delta V$ for adjacent data points. The peaks labeled *A*, *C*, and *D* in Fig. 3 correspond to the coexistence ranges: dilute stage-1–stage-4; stage-3–stage-2*L*; and stage-2*L*–stage-2, respectively, as seen by comparing to Fig. 2. In a previous work[20] the voltage resolution (0.01 V in Ref. 20) was 10 times poorer than in the present work and we did not observe *C*. The peaks labeled *B* are not understood and will be discussed further later.

Using *in situ* x-ray diffraction, we examined the structural changes taking place in different regions of the Li/graphite voltage curve. The experiments reported here were done while Li was being inserted into the carbon; similar results were obtained during deintercalation. Figure 4 shows portions of x-ray scans in the region of the graphite (002) peak taken for $V > 0.230$ V, above the first plateau in Fig. 2. The (002) peak corresponds to the average spacing between carbon layers. For $V > 0.230$ V, this peaks shifts smoothly to lower angle as the cell voltage decreases (as Li intercalates within the carbon). This shift corresponds to an increase of the (002) plane spacing due to the presence of Li between the layers. All the Bragg peaks arising from the intercalated graphite can be indexed assuming that it is a single phase at each voltage (Li concentration), but whose x axis varies smoothly with voltage. No evidence of superlattice peaks indicative of staged phases were observed for $V > 0.230$ V. This evidence, coupled with the smooth variation of $V(x)$ for $V > 0.230$ V proves that Li is intercalated uniformly

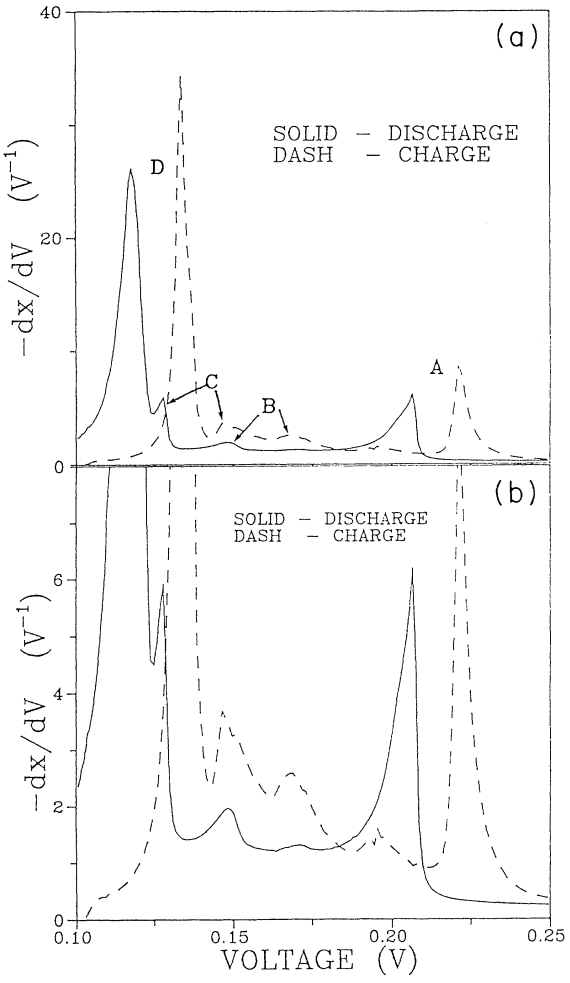

FIG. 3. $-(dx/dV)_T$ vs V for the data of Fig. 2. The data in (b) is the same as in (a) except plotted on an expanded vertical scale. The peaks labeled *A*, *B*, *C*, and *D* in (a) are described in the text.

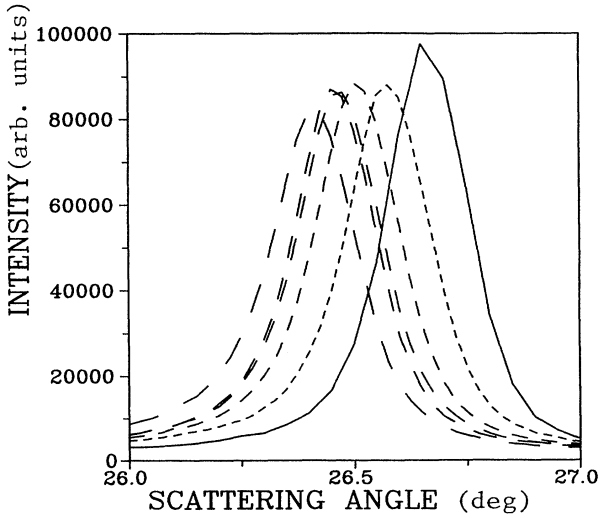

FIG. 4. X-ray intensity vs scattering angle (Cu $K\alpha$ radiation) for the (002) region of Li_xC_6 in the dilute stage-1 phase measured by *in situ* diffraction at 21 °C. From the right, the scans were measured at the following cell voltages: 2.00 (fresh cell), 0.400, 0.295, 0.257, 0.257, and 0.230 V. One of the scans at 0.257 V was measured as the cell voltage was stepped down, and the other while the cell voltage was stepped up.

within host at these concentrations forming a dilute stage-1 phase.

Next we examined the plateau in $V(x,T)$ near 0.2 V. Figure 5(a) shows the region near the dilute stage-1 (002) peak and the stage-4 (004) peak. Figure 5(b) shows one area where a stage-4 superlattice peak [in this case, the (005) peak] is expected to appear. [The average layer spacing of a stage-n phase is given by the d spacing of the ($00n$) planes, except for graphite and dilute stage 1, where the (002) plane spacing is used. This is because a stage-n phase contains n carbon planes per unit cell, except for the dilute stage-1 phase, which probably contains two carbon layers in $ABABAB\ldots$ stacking like graphite. Superlattice peaks for staged phases appear because the intercalant is only present between every nth pair of carbon planes for stage n. In our notation, ($00l$) peaks, which are observable only because of the staging, are called superlattice peaks. The Miller indices for the ($00l$) superlattice peaks of a stage-n phase are given by all integers l such that l is not an integral multiple of n.] As the voltage decreases and we move across the plateau, a coexistence between the dilute stage-1 phase and the stage-4 phase is clearly observed. In the third scan displayed in Fig. 5(a) (collected at 0.202 V), two peaks, corresponding to the average layer spacings of the two coexisting phases, are observed. The phase which forms at the lower voltage is the stage-4 phase because the (005) peak of the stage-4 phase appears exactly where expected

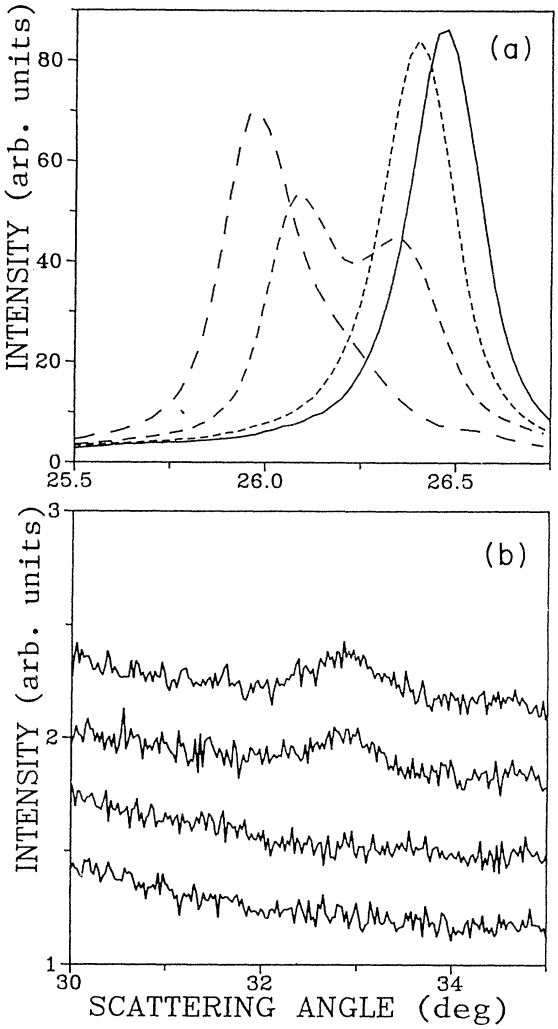

FIG. 5. *In situ* diffraction results for a Li/Li_xC_6 cell in the dilute stage-1–stage-4 coexistence region. From the right in (a) and from the bottom in (b), the scans were measured at the following voltages: 0.257, 0.210, 0.202, and 0.200 V. (a) shows the Bragg peaks corresponding to the average spacing between carbon planes and (b) shows the stage-4 (005) peak. [The scans in (b) have been offset vertically by 0.3 for clarity.]

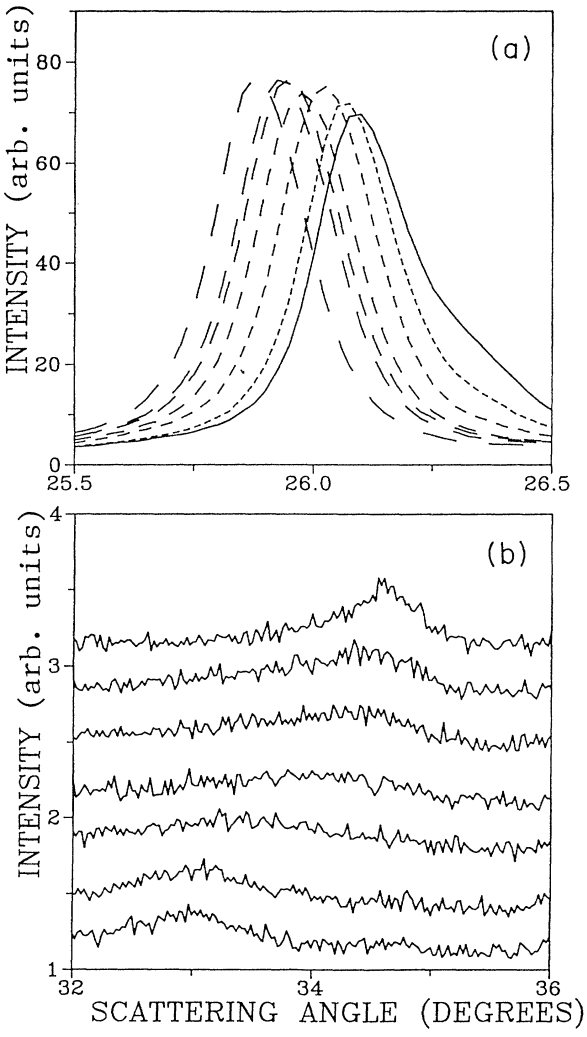

FIG. 6. *In situ* diffraction results in the stage-4–stage-3 transition region. From the right in (a) and from the bottom in (b), the scans were measured at the following voltages: 0.200, 0.190, 0.185, 0.180, 0.175, 0.170, and 0.160 V. (a) shows the Bragg peak corresponding to the average spacing between carbon planes and (b) shows the stage-4 (005) peak (near 33°) and the stage-3 (004) peak (near 34.7°). [The scans in (b) have been offset vertically by 0.3 for clarity.]

[as shown in Fig. 5(b)].

As further Li is added, we next move into a region where the cell voltage varies appreciably with x. Figure 6 shows x-ray scans taken for $0.201\ \text{V} > V(x,T) > 0.159\ \text{V}$, all at voltages greater than peak B (on discharge) in Fig. 3. Figure 6(a) shows that the peak corresponding to the average layer spacing shifts smoothly as Li is added. Figure 6(b) is a scan which simultaneously probes the presence of the (005) peak of the stage-4 phase and the (004) peak of the stage-3 phase. There appears to be a smooth shift of the superlattice intensity from the state-4 position to the stage-3 position as Li is added. This would be expected if the material is composed of a fraction, f, of stage-4 packets randomly mixed with a fraction, $1-f$, of stage-3 packets.[23] As Li is inserted, f changes from 1 to 0 and the superlattice peak would change from stage 4 (005) to stage 3 (004) in a continuous manner much like that observed. We do not fully understand the stage-4 to stage-3 transition, but emphasize that it is markedly different from the dilute stage-1 to stage-4 transition described above, the stage-3 to stage-2L and the stage-2L to stage-2 transition will be described next. The latter three transitions all show clear two-phase coexistence regions by x-ray diffraction and plateaus in $V(x,T)$ while the stage-4 to -3 transition does not.

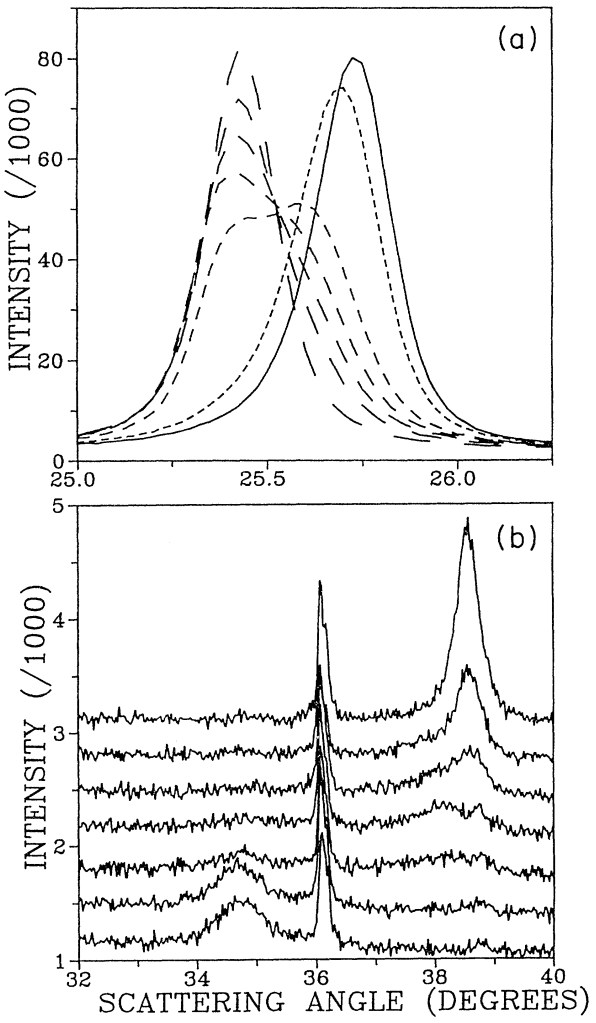

FIG. 7. *In situ* diffraction results in the stage-3–stage-2L and stage-2L–stage-2 regions. From the right in (a) and the bottom in (b), the scans were measured at the following voltages: 0.130, 0.125, 0.120, 0.118, 0.115, 0.113, and 0.100 V. (a) shows the Bragg peaks corresponding to the average spacing between carbon layers and (b) shows the stage-3 (004) peak (near 34.7°) and the stage-2 (003) peak (near 38.7°). The peak near 36.1° is from the metallic Li anode in the cell. The data in (b) have been offset vertically by 0.3 for clarity.

Figure 7 shows *in situ* x-ray-diffraction data collected for $0.131\ \text{V} > V(x,T) > 0.99\ \text{V}$ as the cell voltage is stepwise decreased. In this range of voltage, the stage-3–stage-2L and stage-2L–stage-2 transitions both occur. Figure 7(a) shows the peak corresponding to the average layer spacing and Fig. 7(b) shows a region of the profile which probes the (004) peak of the stage-3 phase and the (003) peak of both stage-2 phases. As Li is added, a clear phase separation is observed in the third scan from the right in Fig. 7(a) and the third scan from the bottom in Fig. 7(b), both measured at 0.120 V. By the fifth scan, the stage-3 phase is absent and only the stage-2L phase is present. By the fifth scan we have moved completely through the peak labeled C in Fig. 3(a). During the next two scans,[6,7] we move through the peak labeled D in Fig. 3(a) and form the stage-2 phase. We have insufficient resolution to distinguish the difference between the average layer spacing of the stage-2 and stage-2L phases and infer the existence of the 2L phase mainly from the presence of both peaks C and D in Fig. 3(a) and from the previous work on the phase diagram of Li_xC_6.[7,8,10]

The previously reported phase diagram for Li_xC_6 shows that the 2L phase disappears below about 260 K.[8,24] We used measurements of $-(dx/dV)_T$ at various temperatures to probe this. Figure 8 shows $-(dx/dV)_T$

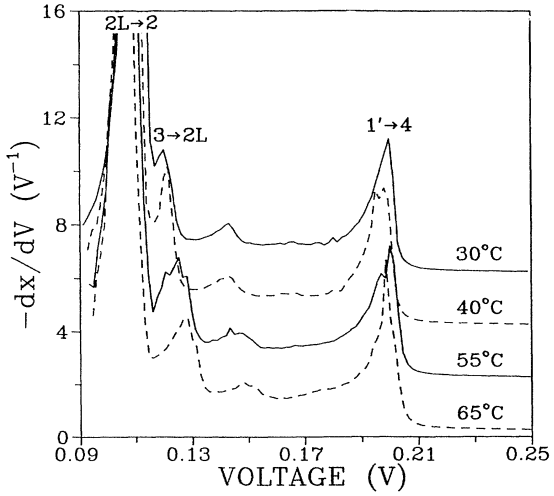

FIG. 8. $-(dx/dV)_T$ vs voltage for a Li/Li_xC_6 cell at temperatures indicated using a discharge current corresponding to a change $\Delta x = 1$ in 200 h. The correspondence between the peaks in $-dx/dV$ and the phase transitions in Li_xC_6 is indicated. The data has been offset vertically by 2.0 V^{-1} for clarity.

plotted versus V measured at 30, 40, 55, and 65 °C for the discharge of a Li/graphite cell using a current where a change, $\Delta x = 1$ in Li_xC_6 occurs in 200 h. The separation between the peaks in $-(dx/dV)_T$, corresponding to the stage-3–stage-2L and the stage-2L–stage-2 transitions, decreases as the temperature decreases. Once these peaks merge into a single peak, as the temperature is further lowered, then a transition directly from stage 3 to stage 2 will occur. Figure 9 shows the separation between the peaks plotted versus temperature. Assuming that the separation varies linearly with temperature, we expect that the 2L phase will disappear below 10°±2 °C. Measurements at 10 °C confirm the absence of the stage-3–stage-2L peak in $-(dx/dV)_T$.

The peaks labeled B in Fig. 3(a) are still a mystery. Our experiments show that this peak is located in a range where Li_xC_6 is in the stage-3 phase. Perhaps this peak is associated with some ordering of the intercalated Li within each occupied layer. Our diffraction experiments do not probe the ($hk0$) reflections well because the graphite electrodes in our cells have been compressed[18] causing ($00l$) reflections to be preferentially favored.

Finally, we constructed some cells using electrodes without Super S Battery Black to probe the width of the dilute stage-1 region. Figure 10 shows $V(x,T)$ for such a cell in the dilute stage-1 region, measured using a current corresponding to $\Delta x = 1$ in Li_xC_6 in 400 h. The single-phase region extends from $x = 0$ to 0.04±0.005 at 30 °C. The results in Fig. 10 agree well with those in Fig. 2 if the contributions of the Super S Battery Black present in the cell of Fig. 2 are taken into consideration. The data of Fig. 2 suggest the single-phase region has a width of $\Delta x = 0.07$. The Super S Battery Black has a total capacity which corresponds to $\Delta x = 0.037$ between 1.4 and 0.01 V. Assuming this capacity to be distributed uniformly over this voltage range,[22] the capacity of the graphite above 0.23 V in the data of Fig. 2 is

$$\Delta x = 0.07 - 0.037 \times 1.2/1.4 = 0.039 ,$$

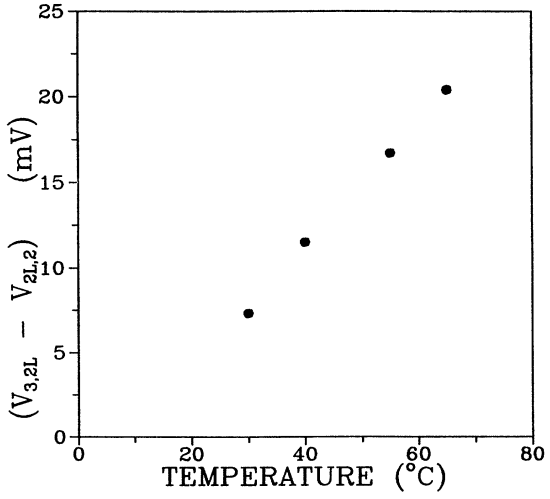

FIG. 9. Separation between peaks in $-(dx/dV)_T$ corresponding to the 3+2L and 2L +2 transitions vs temperature.

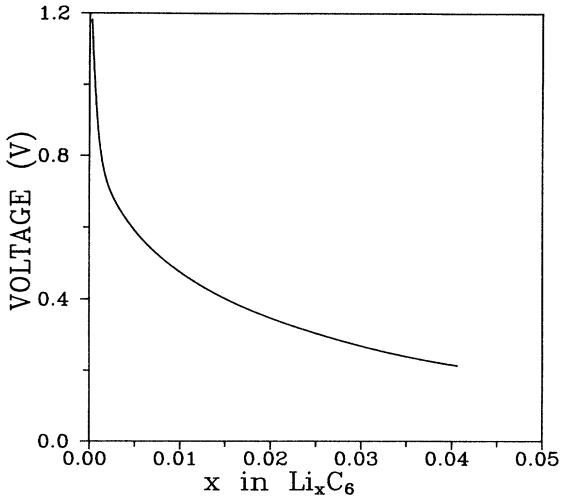

FIG. 10. Voltage vs x for a Li/Li_xC_6 cell at 30 °C without Super S Battery Black in the electrode for x in the dilute stage-1 region. The current corresponds to a change $\Delta x = 1$ in 400 h.

in good agreement with Fig. 10.

To construct the Li_xC_6 phase diagram shown in Fig. 11, we used the data of Figs. 2, 3, and 8–10 as well as the x-ray information presented above. For $0.5 < x < 1.0$, a coexistence between the stage-2 and stage-1 phases is observed. The single-phase stage-2L and stage-2 phases are narrow, of maximum width $\Delta x = 0.03$; these have been denoted as line phases in Fig. 11. There is little temperature dependence in the phase diagram apart from the disappearance of the 2L phase below 10 °C. We have la-

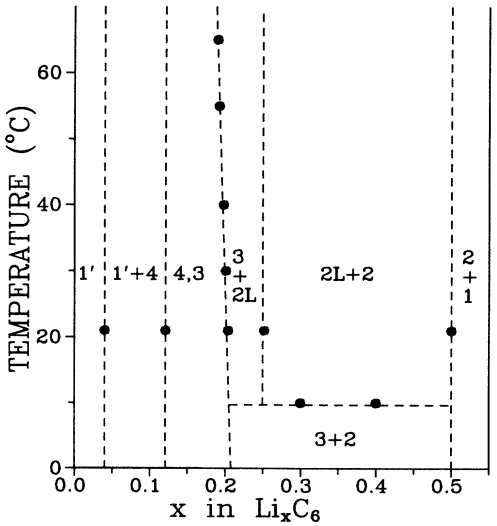

FIG. 11. The phase diagram of Li_xC_6 in the range 0 °C $< T <$ 70 °C. The phase designations are described in the text. Data points are plotted where the error in x and T of the phase boundary is less than ±0.015 and ±2 °C, respectively. Elsewhere, the errors in x at a given T are estimated to be less than ±0.03.

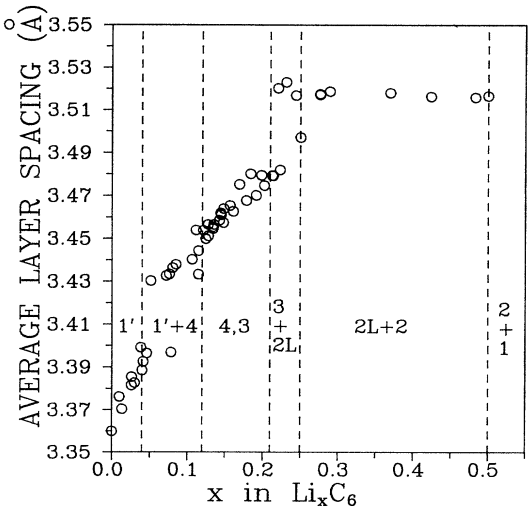

FIG. 12. Variation of the average layer between carbon planes as a function of x in Li_xC_6 measured at 21 °C. The phase diagram information from Fig. 11 for 21 °C is superimposed.

beled the region of the phase diagram corresponding to stages 3 and 4 as "3,4." At the extreme left of the "3,4" phase, Li_xC_6 is pure stage 4 while at the right it is pure stage 3. In the discussion regarding Fig. 6, we showed that distinct coexisting phases were not observed during the stage-3–stage-4 transition and that the transition appeared to be continuous. This is in disagreement with the results reported in Ref. 8 (see Fig. 14 in that reference) where a clear two-phase coexistence region is observed between stage 3 and stage 4 LiC_{62} ($Li_{0.097}C_6$) as the temperature is increased, although the temperatures are not given in that reference. We emphasize that further work is needed to fully understand the stage-3–stage-4 transition.

The major differences between our Li_xC_6 phase diagram and those previously determined (for example, see Fig. 3.6 in Ref. 24) are now summarized. First, the dilute stage-1 phase, labeled 1′ in Fig. 11, extends to from $x=0$ to 0.04 at 300 K, and does not have zero width as implied by previous work. Second, the width of the two-phase coexistence region between the stage-2L phase and the stage-2 phase is much larger than implied by previous work. Third, the stage-3–stage-4 transition has markedly different behavior than the other transitions which are all clearly first-order transitions. Finally, there is no evidence for the stability of phases with a stage index greater than 4 above 10 °C.

The lattice expansion induced by the intercalant can be used to probe the elastic energies associated with intercalation.[25,26] Furthermore, phenomenological models used to predict the lattice expansion of Li_xC_6 have suffered in that precision data for comparison has not been available.[26] Figure 12 shows the average spacing between carbon layers plotted as a function of x from our *in situ* experiments. The regions of the phase diagram for 21 °C from Fig. 11 have been indicated in Fig. 12. In the two-phase regions, two sets of Bragg peaks are observed except in the $2L+2$ region where we cannot resolve the Bragg peaks from each phase. The layer spacing for stage-1 LiC_6 from *in situ* experiments has been reported previously.[20]

DISCUSSION

The qualitative features of our phase diagram and that determined for Li_xC_6 previously (e.g., see Ref. 8) are similar. Theories for the phase diagram of Li_xC_6 require accurate experimental data for comparison. We have now provided an accurate phase diagram determination, although only within a narrow temperature range. Equally important are the measurements of the voltage of Li/Li_xC_6 cells which we have presented. These are a direct measure of the variation of the chemical potential of the intercalated Li within the graphite as a function of x.[13] Any theory for the phase diagram of Li_xC_6 based on lattice-gas models allows for the calculation of this chemical potential variation. Clearly, if a theory is to be considered reasonable, it must reproduce not only the phase diagram, but also the chemical potential variation. It is our opinion that the current theories[25,27–29] are unable to do both. We are now exploring methods to improve the theoretical description of intercalation in Li_xC_6.

The electrochemical methods outlined here are very powerful methods for obtaining phase diagram information. However, the use of liquid electrolytes in Li/Li_xC_6 cells limits the temperature range we can probe. It is our opinion that experiments using solid polymer electrolytes are warranted because the range of cell operation can be extended up to at least 150 °C. The stage-3–stage-4 transition in Li_xC_6 could then be studied under conditions where the Li diffusion is much faster. If kinetics play a role in the apparent complexity of this phase transition, then this approach may allow the separation of the kinetic effects from the equilibrium thermodynamics.

ACKNOWLEDGMENTS

We thank the Natural Sciences and Engineering Research Council of Canada and Moli Energy (1990) Ltd. for funding. Moli Energy (1990) Ltd. performed the vacuum distillation of the electrolyte solvents. Discussions with W. R. McKinnon regarding this work were useful.

[1]R. Juza and V. Wehle, Nature (London) **52**, 560 (1965).
[2]M. Bagoin, D. Guerard, and A. Herold, C. R. Acad. Sci. Ser. C **262**, 557 (1966).
[3]D. Geurard and A. Herold, C. R. Acad. Sci. Ser. C **275**, 571 (1972).
[4]P. Delhaes and J. P. Manceau, Synth. Met. **2**, 277 (1980)
[5]J. E. Fischer, C. D. Fuerst, and K. C. Woo, Synth. Met. **7**, 17 (1983).
[6]J. E. Fischer and H. J. Kim, Synth. Met. **12**, 137 (1985).
[7]J. E. Fischer and H. J. Kim, Synth. Met. **23**, 121 (1988).
[8]J. E. Fischer, in *Chemical Physics of Intercalation,* edited by A. P. Legrand and S. Flandrois (Plenum, New York, 1987).

[9]H. J. Kim, A. Magerl, J. L. Soubeyroux, and J. E. Fischer, Phys. Rev. B **39**, 4760 (1989).
[10]K. C. Woo, H. Mertwoy, J. E. Fischer, W. A. Kamitakahara, and D. S. Robinson, Phys. Rev. B **27**, 7831 (1983).
[11]J. R. Dahn and W. R. McKinnon, J. Electrochem. Soc. **131** 1823 (1984).
[12]J. R. Dahn, W. R. McKinnon, and S. T. Coleman, Phys. Rev. B **31**, 484 (1985).
[13]W. R. McKinnon and R. R. Haering, in *Modern Aspects of Electrochemistry,* edited by R. E. White, J. O'M. Bockris, and B. E. Conway (Plenum, New York, 1983), No. 15, p. 235.
[14]J. R. Dahn, M. A. Py, and R. R. Haering, Can. J. Phys. **60**, 307 (1982).
[15]A. N. Dey and B. P. Sullivan, J. Electrochem. Soc. **117**, 222 (1970).
[16]Y. Takada, R. Fujii, and K. Matsuo, Tanso **114**, 120 (1983).
[17]M. Arakawa and J. Yamaki, J. Electroanal. Chem. **219**, 273 (1987).
[18]R. Fong, U. Von Sacken, and J. R. Dahn, J. Electrochem. Soc. **137**, 2009 (1990).
[19]J. R. Dahn and D. P. Wilkinson, U.S. Patent Application 602 497 (pending).
[20]J. R. Dahn, R. Fong, and M. J. Spoon, Phys. Rev. B **42**, 6424 (1990).
[21]W. Ruland, Acta Crystallogr. **18**, 992 (1965).
[22]R. S. McMillan (unpublished).
[23]S. Hendricks and E. Teller, J. Chem. Phys. **10**, 147 (1942).
[24]G. Kirczenow, in *Graphite Intercalation Compounds I,* Vol. 14 of *Springer Series in Materials,* edited by H. Zabel and S. A. Solin (Springer-Verlag, New York, 1990).
[25]J. R. Dahn, D. C. Dahn, and R. R. Haering, Solid State Commun. **42**, 179 (1982).
[26]J. E. Fischer and H. J. Kim, Phys. Rev. B **35**, 3295 (1987).
[27]S. A. Safran, Phys. Rev. Lett. **44**, 937 (1980).
[28]D. P. DiVincenzo and T. C. Koch, Phys. Rev. B **30**, 7092 (1984).
[29]S. E. Millman and G. Kirczenow, Phys. Rev. B **28**, 3482 (1983).